A SIMPLE ANALYSIS OF HELICAL SLOW-WAVE STRUCTURE LOADED BY DIELECTRIC EMBEDDED METAL SEGMENTS FOR WIDEBAND TRAVELING-WAVE TUBES

R. Seshadri

Microwave Tube Researach and Development Centre
Bangalore-560013, India

S. Ghosh

Bharat Electronics
Bangalore-560013, India

A. Bhansiwal and S. Kamath

Microwave Tube Researach and Development Centre
Bangalore-560013, India

P. K. Jain

Centre for Research in Microwave Tubes
Department of Electronics Engineering
Institute of Technology
Banaras Hindu University
Varanasi-221005, India

Abstract—A simple field analysis was developed for helical slow-wave structure symmetrically supported by rectangular shaped discrete dielectric support rods partially embedded in the metal segments projecting radially inward from a metal envelope for wideband traveling-wave tubes. The tape helix model was used for the prediction of the dispersion relation and the interaction impedance characteristics. The closed form simplified expressions are obtained by combining the tape model dispersion relation for free-space helix and the dielectric loading factor obtained for the loaded helix in the sheath model. The dispersion characteristics and the interaction impedance characteristics obtained by the present analysis were compared with other more

Corresponding author: P. K. Jain (pkjain.ece@itbhu.ac.in).

involved analytical method reported in the literature for the similar helical slow-wave structure and found to be in close agreement. The present analytical results were also validated against HFSS simulation with an agreement within 5% for both the characteristics for a wide range of structure parameters. An appropriate choice of the structure parameters (helix thickness, height of the metal segments, material of the dielectric support rods, wedge segments angle and helix pitch) provided the phase velocity varying with frequency corresponding to flat to negative structure dispersion with an appreciable interaction impedance values over a wide frequency band. The present analysis enjoys simplicity and establishes the potential of the proposed helical interaction structure for its employment in wideband traveling-wave tubes.

1. INTRODUCTION

Traveling-wave tubes (TWTs) find wide range of applications as microwave/millimetre-wave power amplifier due to their unique combination of power gain and bandwidth. Today's electronic warfare (EW) systems like electronic counter measure (ECM) and electronic counter counter measure (ECCM) are dependent on wideband helix TWTs for their wideband capability. A wideband TWT universally uses helical slow-wave structure (SWS) as the interaction structure due to its non-resonant behaviour and consequent wide bandwidth potential [1–13]. The bandwidth and other performance like gain efficiency etc. of the helix TWT can be improved further by suitably tailoring the design of the helical SWS.

In a practical TWT, the helix is supported by a number of dielectric support rods of circular or rectangular cross section and the entire assembly is enclosed in a metal envelope. Discrete dielectric support rods geometry of the SWS, which usually differ from the wedge shape, causes an inhomogeneous loading of the helix [1–7]. The metal segments/vanes projecting radially inwards from the metal envelope causes anisotropic loading of the SWS [8–10]. Both inhomogeneous and anisotropic loadings can be used to control the dispersion of the helical SWS [8–16]. Wideband high gain helix TWTs utilize both types of loading separately as well as simultaneously [9–13]. For wide device bandwidth one requires flat to negative dispersion in order to realize wideband synchronism between DC electron beam velocity and RF phase velocity [2]. Interaction impedance is another device parameter which has to be monitored simultaneously to have its significantly large value and has direct relevance to the gain of the device.

The inhomogeneous loading controls the helix dispersion, but

in order to flatten the shape of the dispersion curve it demands heavy dielectric loading thereby causing reduction in the value of the interaction impedance of the helical SWS. Using anisotropic loading one can control the dispersion without serious reduction of the interaction impedance values. Incorporating inhomogeneous and anisotropic loading simultaneously in the structure one can achieve flat to negative dispersion along with reasonably high interaction impedance values of the helical SWS.

In this paper, the authors have considered a practical wideband helical SWS where the helix is supported by three rectangular dielectric support rods partially embedded in the metal segments and the whole enclosed in a metal envelope (Fig. 1). This structure has merits not only from electromagnetic considerations but also from mechanical considerations in that the structure is thermally rugged, and easy to be fabricated by inserting the dielectric rod and metal segment assembly into the metal envelope. The similar structure has been analyzed by Lei et al. [11] using a tape helix model which, though it is rigorous, is involved and cumbersome. In the present paper, a simple analysis for this structure is presented in the tape helix model (THM) by incorporating into the THM analysis of a free-space helix [17] the dielectric loading factor (D_{LF}) obtained by a simpler sheath helix model (SHM) analysis of a loaded helix [2, 3, 6, 7]. The effect of segment projecting radially inward from the metal envelope is taken by considering that the axial electric field gets shielded at the metal segment tips, where as the azimuthal electric field reaches upto the overall metal envelope [9]. To take into account the effect of width and angular thickness of the metal segments, penetration of
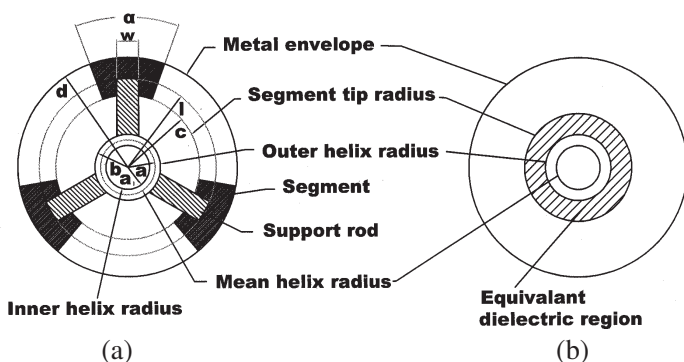

Figure 1. Cross-section of the helical structure with dielectric supports embedded in the segmented metal envelope (a) and its physical equivalent structure model for analysis (b).

axial electric field beyond inter-segment region has been also considered in terms of SWS parameters. The analysis gives simpler closed form expressions for the prediction of both the dispersion and the interaction impedance characteristics of the structure (Section 2). The structure is also simulated using commercially available simulation code Ansoft HFSS [18] (Section 3). The results of the present analysis are compared with those reported by Lei et al. [11] as well as simulation (Section 4). The dependence of the dispersion characteristics and interaction impedance on the various structure parameters is also studied for design optimization.

2. ANALYSIS

The helical slow-wave structure under study (Fig. 1) consists of a helix supported by three rectangular-shaped discrete dielectric support rods partially embedded in the metal segments, the whole enclosed in a metal envelope. The rectangular supports deviating from the simple wedge geometry and the metal segments make the structure inhomogeneous and anisotropic, respectively. For the analysis, in the structure model (Fig. 1(b)), the rectangular-shaped discrete dielectric support rods are azimuthally smoothed out into a single (or a number of) continuous dielectric tube regions, between the helix and the metal segments tip ($b \leq r \leq c$) of an effective permittivity value ε'_r which is found from the relative volume of the dielectric support rods in the structure [1–3]. For practical helical SWS, the dielectric support rods are usually made of APBN (anisotropic pyrolytic boron nitride $\varepsilon_r = 5.1$), quartz ($\varepsilon_r = 3.78$), beryllia ($\varepsilon_r = 6.65$). Their effective dielectric constant is low and also the radial variation of effective dielectric constant value is small, consequently its effect on the electromagnetic performance of the helical SWS is found to be negligible. Hence, for such dielectric helix supports rods one can safely replace the discrete dielectric supports into a single continuous dielectric tube of an equivalent effective dielectric constant. However, for the case of higher permittivity dielectric supports as well as for higher accuracy, discrete dielectric support region can be replaced into a number of effective dielectric tube regions [2, 7]. The number of such tubes can be increased upto the desired accuracy in the result. Here, for the helical structure considered, we have taken 'a' is the mean helix radius, 'b' is the helix outer radius, 'c' is the segment tip radius, 'd' is the metal envelope radius, 'α' is the metal segment angle, 'w' is the width of the dielectric rod, 'θ_a' is the sector of the angle of the non-segment region.

The helical SWS (Fig. 1(a)) has been replaced here by an

equivalent structure model (Fig. 1(b)) for the analysis which essentially makes the problem as a boundary-value problem involving the boundaries between four continuous regions: (i) the free-space region inside the helical sheath of mean helix radius a ($0 \leq r \leq a$), (ii) the free-space region between the helical sheath (equal to mean helix radius) and the beginning of the dielectric support (equal to the outer helix radius) which is usually considered to account for the helix wire/tape thickness ($a \leq r \leq b$), (iii) the continuous, homogeneous dielectric tube region of equivalent relative permittivity ε_r' to account for the discrete dielectric support rods ($b \leq r \leq c$), and (iv) the region between the tips of the metal segment and the overall cylindrical metal envelope ($c \leq r \leq d$).

For the region (iv) of the structure model (Fig. 1(b)), one may take resort to two approaches to account for the effect of the metal segments (Fig. 1). In the first of these approaches [9], for the region (iv) in which metal segment is present as a free space region where the axial electric field "sees" the segments and gets shielded at the metal segment tips ($r = c$), while the azimuthal electric field does not "see" the segments and reaches upto the overall metal envelope ($r = d$) [9]. The model is valid for a large number of thin segments. In the second approach, the field analysis considering angular harmonics is used to predict the axial electric field penetration in the inter-segment region (unless it is reduced by an arbitrarily chosen factor $1/e$ from its value at the metal segment tip ($r = c$)), which in turn is interpreted to predict a modified value of the metal segment tips radius $r = c'$ where the axial electric field could be considered as shielded and then using the modified radius of metal segment it is analyzed as per first approach. We have used the second approach in the present analysis.

The effect of permittivity for the portion of dielectric embedded into the metal segment groove ($c \leq r \leq l$) is neglected in the present model, since the axial field components became null at the metal segments tip ($r = c$) and almost negligible electromagnetic field will penetrate in this portion of the dielectric ($c \leq r \leq l$) [9]. Hence, effect of the groove in the metal segments as well as the dielectric present there is ignored, since it will not affect the electromagnetic behavior of the structure. Furthermore, the presence of the angular periodicity in region (iv) (inter-segment region) of the helical SWS would give rise to the angular harmonics in the structure [8–10]. The structure is field-analyzed in the tape-helix model to account for the effect of axial space harmonics, arising from the space periodicity of the helix, which makes the analysis more rigorous and accurate.

2.1. Dispersion Relation

The helical structure (Fig. 1) is field analyzed here to find its dispersion relation and interaction impedance [1–9]. The analysis of a loaded helix in the conventional tape model is quite encumbered [5]. Hence, in order to find out the dispersion relation of a loaded helix in tape model, a simplified approach reported elsewhere as 'heuristic approach' [3, 4, 6] has been followed here. In this approach first the dispersion relation of a loaded helix in the sheath helix model (SHM) obtained using the relevant field expressions and boundary conditions [2, 3] and the dispersion relation of a helix in the tape helix model (THM) in free-space is obtained using the relevant field expressions and boundary conditions for this case [5, 6]. Then utilizing both of these dispersion relations [3–6], dispersion relation of a loaded helix in the tape model is achieved. Hence, to obtain the dispersion relation of the loaded helical structure under consideration, first the dielectric loading factor (D_{LF}), as a function of structure parameters, is obtained for a loaded helix in the SHM. Then, the dispersion relation of free-space helix in the THM is recalled [13]. Finally, inserting the dielectric loading factor D_{LF}, obtained from the dispersion relation of a loaded helix in SHM, into the dispersion relation of a free-space helix in tape model ($D_{LF} = 1$ for the free-space helix), the dispersion relation for a loaded helix in the tape-helix model is obtained. This "heuristic approach" repeatedly yields the same results as those obtained using involved analysis in the tape-helix model for the loaded helical SWS [3–6].

For the purpose of the field analysis of the structure in the sheath-helix model, the expressions for the electric and magnetic field intensities in the four different regions of the structure can be written, for the azimuthally symmetric ($\partial/\partial\theta = 0$) mode (in the cylindrical coordinates), to appreciate that there exist, in general, four field constants in each of the four regions of the structure [2, 3]. Thus, there are $16 (= 4 \times 4)$ field constants (considering these four regions) out of which, however, two become zero to satisfy the condition that the fields are to be finite at the axis ($r = 0$) of the structure, giving 14 non-zero field constants. Further, the relevant electromagnetic 14 boundary conditions for the problem are: the four tape helix boundary conditions at the mean helix radius [17] at $r = a$, four boundary conditions at each of the two dielectric tube interfaces corresponding to the continuity of the tangential components of electric and magnetic field intensities, and two boundary conditions that the tangential components of the electric field intensity are null at the metal envelope ($r = c$) [2, 3]. Substituting the field expressions into these 14 boundary conditions, one obtains 14 equations in 14 field constants. The condition for the non-trivial solution of these equations will then lead to the following

dispersion relation of the structure (Fig. 1) in the sheath-helix model after a little algebraic manipulation:

$$(\gamma a)^2 \left(I_0\{\gamma a\} K_0\{\gamma a\} \right) D_{LF,0} + (ka \cot \psi)^2 \left(I_0'\{\gamma a\} K_0'\{\gamma a\} \right) = 0 \quad (1)$$

with

$$D_{LF,0} = \left(1 + \frac{M_{0,1} I_0\{\gamma a\}}{N_{0,1} K_0\{\gamma a\}} \right) \left(1 + \frac{M_{0,2} I_0'\{\gamma a\}}{N_{0,2} K_0'\{\gamma a\}} \right)^{-1}$$

as the dielectric loading factor of the structure. Here, $M_{0,1}$ $M_{0,2}$ $N_{0,1}$ and $N_{0,2}$ are functions of the structure parameters and are obtained by putting $m = 0$ in the expressions (2) for $M_{m,1}$ $M_{m,2}$, $N_{m,1}$ and $N_{m,2}$ given below:

$$\left.\begin{aligned}
M_{m,1} &= - \lfloor K_m'\{\gamma b\} \left(P_{m,1}, I_m\{\gamma b\} - K_m\{\gamma b\} \right) \\
&\quad + \varepsilon_{r,3}' K_m\{\gamma b\} \left(P_{m,1} I_m\{\gamma b\} - K_m'\{\gamma b\} \right) \rfloor \\
N_{m,1} &= \lfloor I_m\{\gamma b\} \left(P_{m,1} I_m\{\gamma b\} - K_m\{\gamma b\} \right) \\
&\quad + \varepsilon_{r,3}' I_m\{\gamma b\} \left(P_{m,1} I_m'\{\gamma b\} - K_m'\{\gamma b) \right) \rfloor \\
M_{m,2} &= - \lfloor K_m\{\gamma b\} \left(K_m\{\gamma b\} - Q_{m,1} I_m\{\gamma b\} \right) \\
&\quad + K_m\{\gamma b\} \left(Q_{m,1} I_m'\{\gamma b\} - K_m'\{\gamma b\} \right) \rfloor \\
N_{m,2} &= \lfloor I_m\{\gamma b\} \left(Q_{m,1} I_m'\{\gamma b\} - K_m'\{\gamma b\} \right) \\
&\quad + K_m\{\gamma b\} \left(K_m\{\gamma b\} - Q_{m,1} I_m\{\gamma b\} \right) \rfloor
\end{aligned}\right\}, \quad (2)$$

where

$$\begin{aligned}
P_{m,1} &= \frac{X_2 K_m\{\gamma c\} - \varepsilon_{r,3}' X_1 K_m'\{\gamma c\}}{X_2 I_m\{\gamma c\} - \varepsilon_{r,3}' X_1 I_m'\{\gamma c\}} \\
\text{and } Q_{m,1} &= \frac{X_5 K_m\{\gamma c\} - X_6 K_m'\{\gamma c\}}{X_5 I_m\{\gamma c\} - X_6 I_m'\{\gamma c\}}.
\end{aligned} \quad (3)$$

Now, the dispersion relation of the helix in free-space, in the tape helix model may be written as [3, 4, 6, 17]:

$$\sum_{m=-\infty}^{\infty} \left[\left(\gamma_m a - \frac{m \beta_m \cot \psi}{\gamma_m} \right)^2 I_m\{\gamma a\} K_m\{\gamma a\} \right.$$

$$\left. + (ka \cot \psi)^2 I_m'\{\gamma a\} K_m'\{\gamma a\} \right] \frac{\sin (\beta_m \delta/2)}{(\beta_m \delta/2)} = 0. \quad (4)$$

Combining (1) and (4), the dispersion relation of the loaded structure under consideration (Fig. 1) in the tape helix model can be written

as [3, 4, 6]:

$$\sum_{m=-\infty}^{\infty} \left[\left(\gamma_m a - \frac{m\beta_m \cot\psi}{\gamma_m} \right)^2 I_m\{\gamma a\} K_m\{\gamma a\} D_{LF,m} \right.$$

$$\left. + (ka\cot\psi)^2 I'_m\{\gamma a\} K'_m\{\gamma a\} \right] \frac{\sin(\beta_m\delta/2)}{(\beta_m\delta/2)} = 0 \qquad (5)$$

with $D_{LF,m} = \left(1 + \frac{M_{m,1}I_m\{\gamma a\}}{N_{m,1}K_m\{\gamma a\}}\right)\left(1 + \frac{M_{m,2}I'_m\{\gamma a\}}{N_{m,2}K'_m\{\gamma a\}}\right)^{-1}$.

Here $\gamma_m = \left(\beta_m^2 - k^2\right)^{0.5}$ is the radial propagation constant, $[\beta_m = \beta_0 + m\cot\psi)/a]$ is the mth harmonic-mode axial propagation constant, ψ and δ are the helix pitch angle and the tape width, respectively. $M_{m,1}$, $N_{m,1}$, $M_{m,2}$, $N_{m,2}$, $P_{m,1}$ and $Q_{m,1}$ are the functions of the structure parameters. $I_{mn}(\gamma r)$, $K_{mn}(\gamma r)$ are the modified Bessel functions of the first and second kind and $I'_{mn}(\gamma r)$, $K'_{mn}(\gamma r)$ are the first order derivative of the Bessel functions. Parameters X_p ($p = 1, 2, \ldots, 10$) appeared in $P_{m,1}$ and $Q_{m,1}$ are defined in Appendix.

The expression of D_{LF} gets modified due to penetration of field in the inter-segment regions as given in (1) or (5) in present analysis. As a first-order approximation, considering only the dominant first angular harmonic component ($m = 1$), the axial electric field in the inter-segment region, normalized with respect to its value at the segment tips, is given by [9]:

$$\frac{E_{zm}\{c+\zeta\}}{E_{zm}\{c\}} = \frac{K_m\{\gamma(c+\zeta)\}I_m\{\gamma d\} - K_m\{\gamma d\}I_m\{\gamma(c+\zeta)\}}{K_m\{\gamma c\}I_m\{\gamma d\} - K_m\{\gamma d\}I_m\{\gamma c\}} = \frac{1}{e}$$

The value of ζ obtained is used to replace c now by $c\prime (= c + \zeta)$ in the expressions and hence the expression (3) defining $P_{m,1}$ and $Q_{m,1}$ appearing in (2) will get modified as:

$$P_{m,1} = \frac{X_2 K_m\{\gamma c'\} - \varepsilon'_{r,3} X_1 K'_m\{\gamma c'\}}{X_2 I_m\{\gamma c'\} - \varepsilon'_{r,3} X_1 I'_m\{\gamma c'\}}$$

$$\text{and } Q_{m,1} = \frac{X_5 K_m\{\gamma c'\} - X_6 K'_m\{\gamma c'\}}{X_5 I_m\{\gamma c'\} - X_6 I'_m\{\gamma c'\}}. \qquad (6)$$

2.2. Interaction Impedance

The Interaction impedance of the structure K, measures the amplitude of the axial electric field available for interaction with the electron beam, a parameter important from the standpoint of the gain and

efficiency of the TWT. K is defined as [1–12]:

$$K = \frac{E_{z,m}^2\{0\}}{2\beta_m^2 \sum\limits_{m=-\infty}^{\infty} P_m} \tag{7}$$

where $E_{z,m}^2\{0\}$ is the mth mode axial electric field intensity at the axis of the helix at $r = 0$ and can be expressed in terms of the field constant $A_{m,1}$. The definition is valid for a thin electron beam and more precisely one should take the square of the axial electric field averaged over the cross section of the electron beam instead of $E_{z,m}^2\{0\}$ [3].

$P_m \,(= P_1 + P_2 + P_3 + P_4 + P_5)$ is the total power propagating down the structure. P_m can be obtained by taking half of the real part of the integration of the complex Poynting vector over the structure cross section. Thus:

$$P_1 = \frac{\pi\beta_m\omega\varepsilon_0}{\gamma_m^2}\left(1 - \frac{\gamma_m^2}{k^2\cot^2\psi}\right)\left(\frac{I_m\{\gamma a\}}{I'_m\{\gamma a\}}\right)^2 E_z^2\{0\} \int\limits_0^a I'^2_m\{\gamma r\}r\,dr,$$

$$P_2 = \frac{\pi\beta_m\omega}{\gamma_m^2}\left[\left(\varepsilon_0 A_2^2 - \mu_0 C_2^2\right)\int\limits_a^b I'^2_m\{\gamma r\}r\,dr - \left(\varepsilon_0 B_2^2 - \mu_0 D_2^2\right)\right.$$
$$\left.\int\limits_a^b K'^2_m\{\gamma r\}r\,dr + 2\left(\varepsilon_0 A_2 B_2 - \mu_0 C_2 D_2\right)\int\limits_a^b I'_m\{\gamma r\}K'_m\{\gamma r\}r\,dr\right],$$

$$P_3 = \frac{\pi\beta_m\omega}{\gamma_m^2}\left[\left(\varepsilon_0\varepsilon'_{r,3}A_3^2 - \mu_0 C_3^2\right)\int\limits_b^c I'^2_m\{\gamma r\}r\,dr - \left(\varepsilon_0\varepsilon'_{r,3}B_3^2 - \mu_0 D_3^2\right)\right.$$
$$\left.\int\limits_b^c K'^2_m\{\gamma r\}r\,dr + 2\left(\varepsilon_0\varepsilon'_{r,3}A_3 B_3 - \mu_0 C_3 D_3\right)\int\limits_b^c I'_m\{\gamma r\}K'_m\{\gamma r\}r\,dr\right],$$

$$P_4 = \frac{\beta_m}{2\gamma_m}\int\limits_{J\frac{2\pi}{3}-\theta_a}^{2\pi/3}\int\limits_c^l\left[B_{41}L_1\left(\frac{\omega\varepsilon_0}{\gamma_m}\beta_{41}L_{10} - \frac{\beta_m n\pi}{\gamma_m^2 r\theta_a}D_{41}L_3\right)\sin^2\chi + D_{41}L_3\right.$$
$$\left.\left\{\left(\frac{\beta_m n\pi}{\gamma_m^2 r\theta_a}B_{41}L_5 - \frac{\omega\mu_0}{\gamma_m}D_{41}L_6\right)\cos\chi - \frac{\omega\mu_0}{\gamma_m}D_{410}L_7\right\}\cos\chi\right]r\,dr\,d\theta,$$

$$P_5 = \frac{\beta_m}{2\gamma_m} \int\limits_{(j-1)\frac{2\pi}{3}+\frac{\alpha-\theta b}{2}}^{(j-1)\frac{2\pi}{3}+\frac{\alpha+\theta b}{2}} \int\limits_c^l \left[B_{42}L_2 \left(\frac{\omega\varepsilon_0\varepsilon'_{r,4}}{\gamma_m} B_{42}L_8 - \frac{\beta_m n\pi}{\gamma_m^2 r\theta_b} D_{42}L_4 \right) \sin^2\xi \right.$$

$$\left. - D_{42}L_4 \left\{ \left(\frac{\beta_m n\pi}{\gamma_m^2 r\theta_b} B_{42}L_2 - \frac{\omega\mu_0}{\gamma_m} D_{42}L_8 \right) \cos\xi - \frac{\omega\mu_0}{\gamma_m} D_{420}L_9 \right\} \cos\xi \right]$$

$$r\,dr\,d\theta.$$

In the above expressions of power P_p, A_p, B_p, C_p and D_p ($p = 1, 2, \ldots$) are the field constants and L_1, L_2, $\ldots$, L_{10} are functions of structure parameters and are defined in Appendix.

3. SIMULATION

The simulation of the helical SWS under consideration (Fig. 1) is carried out using commercially available 3D Electromagnetic software, Ansoft HFSS [18]. This high frequency structure simulator (HFSS) software is based on the finite element method (FEM). The helical structure is an axially periodic structure and for the time efficient simulation, the helical slow-wave structure can be truncated for a single period. A single period structure length and master-slave boundary is adapted in the present simulation model [18]. A master-slave boundary related by the expression $E_M = E_S \exp(j\phi)$ is used, where E_M is the electric field boundary of the master and E_S is the electric field boundary of the slave and ϕ the phase factor are used for getting the eigen frequencies.
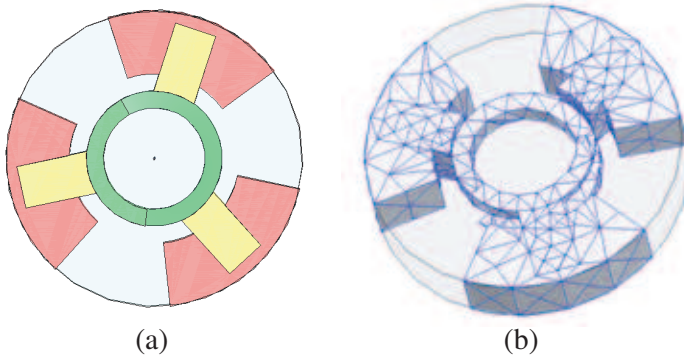

Figure 2. Simulation model of helical slow-wave structure (a) and with meshes (b).

   The eigenmode solver is used to compute the frequencies for the phase difference specified between the master and slave boundaries resulting in different sets of eigenfrequencies for varying phase differences. The dispersion relation is calculated using the expression $v_p = \omega/\beta$ where ω is the angular frequency, β is the axial propagation constant. The onaxis electric field strength $E_{z0}(0)$ and the total power propagating down the structure, is obtained through the field calculator of the HFSS software. The post processor gives the axial electric field and power propagating through the structure. The calculator of the post processing section is made up of a stack of registers, each of which can hold field quantities on which a quantity is to be calculated. The simulated value of the interaction impedance K of the helical SWS is obtained through a statement written to realize the expression (7).

   In the present HFSS simulation approach where helical structure is truncated for a single period and gives a time efficient simulation. The computation time is very short using the ordinary PC.

4. RESULTS AND DISCUSSION

The present simplified approach has been reportedly yielded in the past for other types of helical structures [11] the results as accurate as those obtained by a complex analysis using the tape-helix model. The results of the present simplified analysis (Section 3) for the helical structure with dielectric supports embedded in the segmented metal envelope have been presented and numerically appreciated in this section (Figs. 3–8). The results with respect to both the dispersion and the interaction impedance characteristics obtained by the present analysis with the help of (5) and (7), respectively (Section 3), have
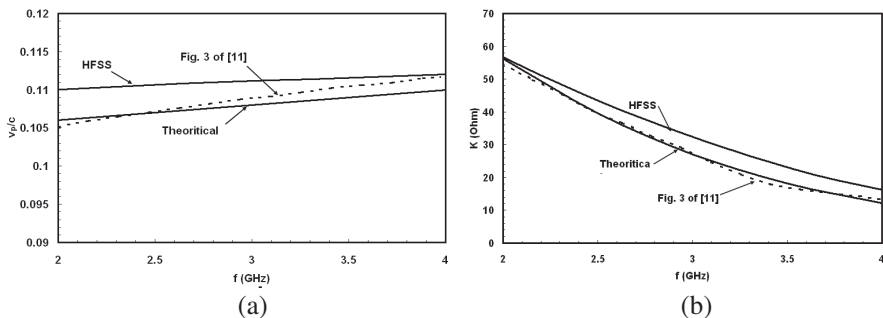

Figure 3. Comparison of dispersion characteristics (a) and interaction impedance (b) with the present analytical results, and the analytical results of Liu et al. [11] as well as with simulation (HFSS) values.
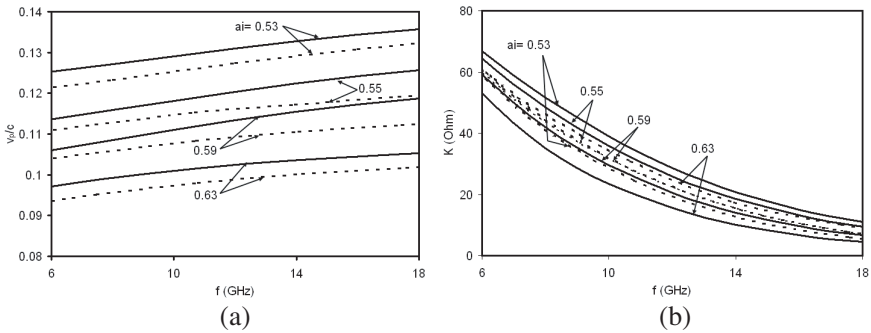
Figure 4. Comparison of theoretical (solid line) and simulated (HFSS) (broken line) results for the phase velocity (a) and interaction impedance (b) versus frequency characteristics, taking the helix inner radius (a_i) as the parameter.
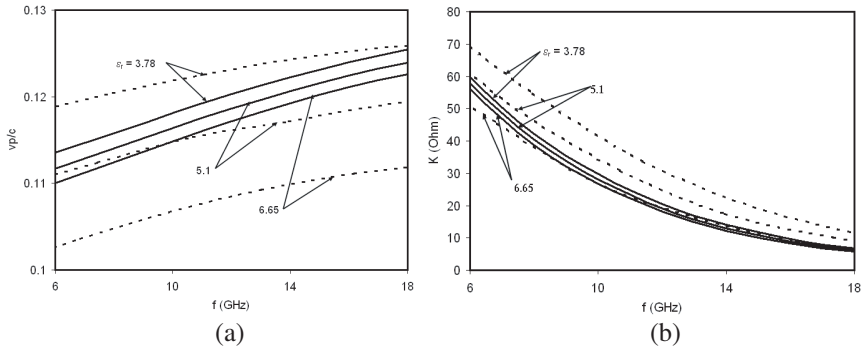

Figure 5. Comparison of theoretical (solid line) and simulated (HFSS (broken line) phase velocity (a) and interaction impedance (b) versus frequency characteristics, taking the tip of the segment as the parameter.

agreed within 5% with those obtained through simulation (using HFSS tool) (Section 4). In the dispersion characteristics, the fundamental-mode propagation constant has been interpreted for the phase velocity v_p.

The results for the normalized phase velocity and the interaction impedance obtained by the present analysis have been compared with the results obtained for the similar structure previously though involved and cumbersome analysis [11]. Fig. 3 show that the dispersion as well as the interaction impedance characteristics obtained using these two analytical results very closely matches to each other and within 3% with those obtained through simulation (using HFSS tool) for the structure parameters reported in [11].
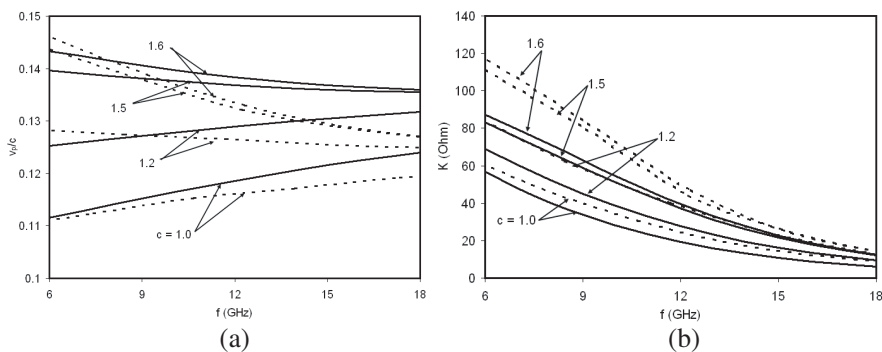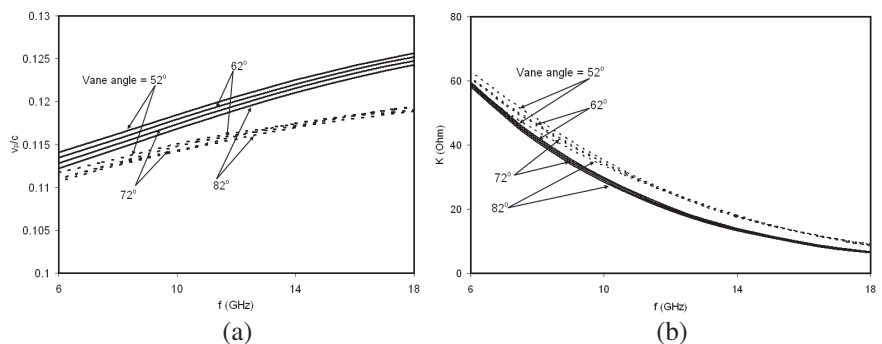
Figure 6. Comparison of theoretical (solid line) and simulated (HFSS (broken line) phase velocity (a) and interaction impedance (b) versus frequency characteristics, taking permittivity of the support material (ε_r) as the parameter.

Figure 7. Comparison of theoretical (solid line) and simulated (HFSS) (broken line) phase velocity (a) and interaction impedance (b) versus frequency characteristics, taking the segment angle as the parameter.

In order to numerically appreciate the broadband potential of the structure, the normalized phase velocity (v_p/c) versus frequency (dispersion) and the interaction impedance versus frequency characteristics have been plotted for the various structure parameters, namely, the helix thickness (helix inner radius (a_i)) (Fig. 4), the position of metal segment tips (c) (Fig. 5), the relative permittivity of the dielectric support rod material (ε_r) (Fig. 6), the segment wedge angle (Fig. 7), and the helix pitch (p) (Fig. 8). The present analytical results have agreed with the simulation results within 5%, for both the dispersion and the interaction impedance (Figs. 4–8). The helical slow-wave structure dimensions, for a practical wideband TWT are taken typically as, mean helix radius (a) $=$ 0.6 mm, helix outer

radius $(b) = 0.8$ mm, metal segment tip radius $(c) = 1.0$ m, metal envelope radius $(d) = 1.75$ mm, helix pitch $(p) = 0.63$ mm, helix tape-width $(\delta) = 0.25$ mm, APBN rectangular helix-support rod width $(w) = 0.5$ mm, vane wedge angle $(\alpha) = 72°$.

It is found from that, with the increase in helix thickness, both analytical and simulated results agree closely with each other and both give negative to positive dispersion (Fig. 4). Also with the increase in vane height, higher permittivity value of the support material, higher wedge angle of the vanes and lower helix pitch, the structure exhibit negative to positive dispersion. However, the analytical results give better agreement at lower frequencies with those obtained by simulation and more so at higher permittivity values of the helix-support materials. The effect of the segment wedge angle (Fig. 7) is not significant in both analytical and simulated results. The interaction impedance of the structure obtained using the present analysis and simulation agree closely throughout a wide range of frequencies, with respect to the variation of the structure parameters.
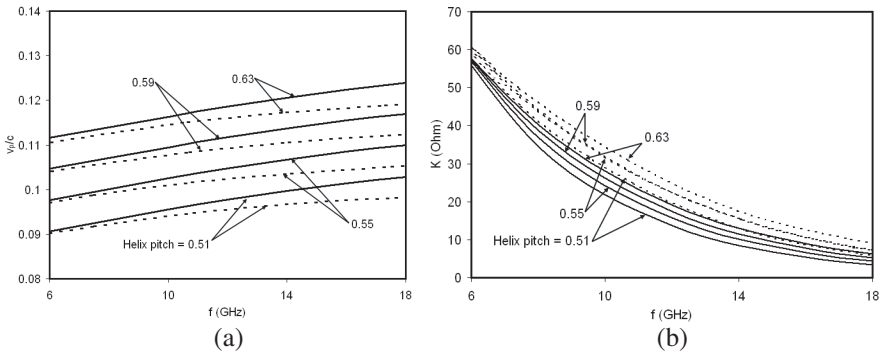

Figure 8. Comparison of theoretical (solid line) and simulated (HFSS (broken line) phase velocity (a) and interaction impedance (b) versus frequency characteristics, taking the helix pitch as the parameter.

5. CONCLUSION

A simple field analysis has been developed for a helical structure supported by rectangular shaped discrete dielectric support rods partially embedded in the metal segments projecting radially inward from a metal envelope, a structure that could be easily fabricated and assembled as well, to be used in the high-gain wideband TWTs. The closed form simplified expressions has been obtained by combining the tape model dispersion relation for free-space helix with the dielectric

loading factor obtained for the loaded helix in the sheath model. The dispersion and interaction impedance characteristics obtained by the present analysis agreed with those obtained by more involved analytical method reported in the literature. The present analytical results were also validated against simulation, using HFSS tool, with an agreement within 5% for both the dispersion and interaction impedance characteristics for a wide range of structure parameters. An appropriate choice of the helical structure parameters provided flat to negative structure dispersion with an appreciable interaction impedance values over a wide frequency band. This establishes the potential of the proposed helical SWS as a high-gain wideband interaction structure. Also, it is hoped that present simple field analysis which retains the rigor of the tape-helix model would be useful in the design and optimization of this helical structure for the development of wideband TWTs.

ACKNOWLEDGMENT

APPENDIX A.

A_p, B_p, C_p and D_p $(p = 1, 2, \ldots,)$ are the field constants and L_1, L_2, $\ldots$, L_{10} are the functions of the structure parameters and are given as follows:

$$A_2 = \frac{M_{m,1} I_{ma} E_z\left(0\right)}{M_{m,1} I_{ma} + N_{m,1} K_{ma}}$$

$$B_2 = A_2 \frac{N_{m,1}}{M_{m,1}}$$

$$A_3 = -\left[\frac{E_z\{0\}}{K_{mb} - P_{m,1} I_{mb}}\right]\left[\frac{P_{m,1} I_{ma}}{M_{m,1} I_{ma} + N_{m,1} K_{ma}}\right][M_{m,1} I_{mb} + N_{m,1} K_{mb}]$$

$$B_4 = -\frac{A_3}{P_{m,1}}$$

$$B_{41} = -\left[\frac{E_z\{0\}}{K_{mb} - P_{m,1} I_{mb}}\right]\left[\frac{I_{ma}}{M_{m,a} I_{ma} + N_{m,1} K_{ma}}\right]$$
$$[M_{m1} I_{mb} + N_{m,1} K_{mb}]\left[\frac{P_{m,1} I_{mc} - K_{mc}}{X_1}\right]$$

$$B_{42} = B_{41} \frac{X_1}{X_3}$$

$$C_1 = -\left(\frac{j\gamma_m}{\omega\mu_0\cot\psi}\right)\left(\frac{I_{ma}}{M_{m,1}I_{ma}}\right)E_z\{0\}$$

$$C_2 = -\left(\frac{j\gamma_m}{\omega\mu_0\cot\psi}\right)\left(\frac{M_{m,2}I_{ma}}{M_{m,2}I_{ma}+N_{m,2}K'_{ma}}\right)E_z\{0\}$$

$$D_2 = C_2\frac{N_{m,2}}{M_{m,2}}$$

$$C_3 = -\left[\frac{Q_{m,1}}{Q_{m,1}I_{mb}-K_{mb}}\right]\left[\frac{j\gamma_m}{\omega\mu_0\cot\psi}\right]\left[\frac{I_{ma}}{M_{m,2}I_{ma}+N_{m,2}K_{ma,}}\right]$$
$$[M_{m,2}I_{mb}+N_{m_2}K_{mb}]E_z\{0\}$$

$$D_3 = -\frac{C_3}{Q_{m,1}}$$

$$D_{4,,1} = -\left[\frac{1}{Q_1I_{mb}-K_{mb}}\right]\left[\frac{j\gamma_m}{\omega\mu_0\cot\psi}\right]$$
$$\left(\frac{I_{ma}}{M_2I_{ma}+N_2K'_{ma}}\right)\left(\frac{M_2I_{mb}+N_2K_{mb}}{X_5}\right)E_z\{0\}$$

$$D_{4,2} = \frac{X_5}{X_7}D_{4,1}$$

where X_v $(v = 1, 2, \ldots, 8)$ are functions of structure parameters and are expressed as:

$$X_1 = \left[K_{n\pi/\theta_a}\{\gamma c\} - \frac{K_{n\pi/\theta_a}\{\gamma l\}}{I_{n\pi/\theta_a}\{\gamma l\}}I_{n\pi/\theta_a}\{\gamma c\}\right]\sin\chi$$

$$X_2 = \left[K'_{n\pi/\theta_a}\{\gamma c\} - \frac{K_{n\pi/\theta_a}\{\gamma l\}}{I_{n\pi/\theta_a}\{\gamma l\}}I'_{n\pi/\theta_a}\{\gamma c\}\right]\sin\chi$$

$$X_3 = \left[K_{n\pi/\theta_b}\{\gamma c\} - \frac{K_{n\pi/\theta_b}\{\gamma d\}}{I_{n\pi/\theta_b}\{\gamma d\}}I_{n\pi/\theta_b}\{\gamma c\}\right]\sin\xi$$

$$X_4 = \varepsilon'_{r,4}\left[K'_{n\pi/\theta_b}\{\gamma c\} - \frac{K_{n\pi/\theta_b}\{\gamma d\}}{I_{n\pi/\theta_b}\{\gamma d\}}I'_{n\pi/\theta_b}\{\gamma c\}\right]\sin\xi$$

$$X_5 = \left[K'_{n\pi/\theta_a}\{\gamma c\} - \frac{K'_{n\pi/\theta_a}\{\gamma l\}}{I'_{n\pi/\theta_a}\{\gamma l\}}I'_{n\pi/\theta_a}\{\gamma c\}\right]\cos\chi$$

$$X_6 = \left[K_{n\pi/\theta_a}\{\gamma c\} - \frac{K'_{n\pi/\theta_a}\{\gamma l\}}{I'_{n\pi/\theta_a}\{\gamma l\}}I_{n\pi/\theta_a}\{\gamma l\}\right]\cos\chi$$

$$X_7 = \left[K'_{n\pi/\theta_b}\{\gamma c\} - \frac{K'_{n\pi/\theta_b}\{\gamma d\}}{I'_{n\pi/\theta_b}\{\gamma d\}}I'_{n\pi/\theta_b}\{\gamma c\}\right]\cos\xi$$

$$X_8 = \left[K_{n\pi/\theta_b}\{\gamma c\} - \frac{K'_{n\pi/\theta_b}\{\gamma d\}}{I'_{n\pi/\theta_b}\{\gamma d\}} I_{n\pi/\theta_b}\{\gamma c\} \right] \cos \xi$$

$$\chi = \frac{n\pi}{\theta_a} \left(\phi - J\frac{2\pi}{3} + \theta_a \right)$$

$$\xi = \frac{n\pi}{\theta_b} \left(\phi - (J-1)\frac{2\pi}{3} + \frac{\alpha - \theta_b}{2} \right).$$

The functions $(L_1, \ldots, L_{10})$ appearing in the expressions of power are as follows:

$$L_1 = X_1/\sin\chi|_{r=c}, \quad L_2 = X_3/\sin\xi|_{r=d}, \quad L_3 = X_6/\cos\chi|_{r=d},$$
$$L_4 = X_8/\cos\xi|_{r=d}, \quad L_5 = X_1/\cos\chi|_{r=d}, \quad L_6 = X_5/\cos\chi|_{r=d},$$

$$L_7 = K'_0\{\gamma r\} - \frac{K'_0\{\gamma l\}}{I'_0\{\gamma l\}} I'_0\{\gamma r\}, \quad L_8 = X_4/\sin\xi]_{r=l},$$

$$L_9 = K'_0\{\gamma r\} - \frac{K'_0\{\gamma d\}}{I'_0\{\gamma d\}} I'_0\{\gamma r\}, \quad L_{10} = X_2/\sin\xi]_{r=l}.$$

REFERENCES

1. Ghosh, S., A. K. Sinha, R. K. Gupta, S. N. Joshi, P. K. Jain, and B. N. Basu, "Space-harmonic effects in helical slow-wave structure — An equivalent circuit analysis," *Progress In Electromagnetics Research*, PIER 30, 85–104, 2001.

2. Ghosh, S., P. K. Jain, and B. N. Basu, "Analytical exploration of new tapered-geometry dielectric-supported helix slow-wave structures for broadband TWT's," *Progress In Electromagnetics Research*, PIER 15, 63–85, 1997.

3. Basu, B. N., *Electromagnetic Theory and Applications in Beam-wave Electronics*, World Scientific, Singapore, 1995.

4. Sinha, A. K., R. Verma, R. K. Gupta, L. Kumar, S. N. Joshi, P. K. Jain, and B. N. Basu, "Simplified tape model of arbitrarily-loaded helical slow-wave structures of a traveling-wave tube," *IEE Proc. PT-H*, Vol. 139, 347–350, 1992.

5. Ghosh, S., P. K. Jain, and B. N. Basu, "Rigorous tape model analysis of inhomogeneously loaded helical slow-wave structures," *IEEE Trans. Electron Devices*, Vol. 44, 1158–1168, 1997.

6. Ghosh, S., A. K. Sinha, S. N. Joshi, P. K. Jain, and B. N. Basu, "A heuristic analysis for a dielectric loaded tape helix considering the non-uniformity of the radial propagation constants over the structure cross sections," *Int. Jour. Electronics*, Vol. 88, 197–213, 2001.

7. Jain, P. K. and B. N. Basu, "The inhomogeneous loading effects of practical dielectric supports for the helical slow-wave structure of a TWT," *IEEE Trans. Electron Devices*, Vol. 34, 2643–2648, 1987.

8. Kravchenko, N. P., L. N. Loshakov, and Y. N. Pchel'nikov, "Computation of dispersion characteristics of a spiral placed in a screen with longitudinal ribs," *Radio Engineering & Electronic Physics*, Vol. 32, 33–39, 1976.

9. Kumar, L., R. S. Raju, S. N. Joshi, and B. N. Basu, "Modeling of a vane-loaded helical slow wave structure for broad-band travelling-wave tubes," *IEEE Trans. Electron Devices*, Vol. 36, 1991–1999, 1989.

10. Paik, S. F., "Design formulas for helix dispersion shaping," *IEEE Trans. Electron Devices*, Vol. 16, 1010–1014, 1969.

11. Lei, W., Z. yang, L. Liao, and P. Liao, "Analysis of a U-shaped vane-loaded helical slow-wave structure for wideband travelling wave tubes," *Int. Jour. Electronics*, Vol. 92, 161–172, 2005.

12. Jung, S. S., C. W. Baik, S. T. Han, S. G. Jeon, H. J. Ha, A. V. Soukhov, B. F. Jia, G. S. Park, H. S. Kim, H. S. Uhm, and B. N. Basu, "Wide-band semivane and heavily dielectric loaded helix traveling-wave tubes," *IEEE Trans. Plasma Science*, Vol. 30, 1009–1015, 2002.

13. Zhu, Z., B. Jia, and Z. Luo, "Calculation of high-frequency characteristics for ridge-loaded helical slow-wave structure," *Proceedings IEEE Int. Vacuum Electronics Conf. (IVEC-2008)*, 113–114, 2008.

14. Kory, C. L., "Validation of an accurate three-dimensional helical slow-wave circuit model," NASA Contract Report 4766, NAS3-27600, March 1997.

15. Zhang, Y., Y. L. Mo, J. Q. Li, and X. L. Zhou "Modelling of finite size vane-loaded helical slow-wave structures," *IEE Proceedings — Microwaves and Antenna Propagation*, Vol. 151, 135–142, 2004.

16. Yang, J., Y. Zhang, X. Cai, and L. Li, "Study on effect of different metallic vane-loaded helix slow-wave structure in travelling-wave tubes," *Jour. Infrared Millimeter Terahertz Waves*, Vol. 30, 611–621, 2009.

17. Sensiper, S., "Electromagnetic wave propagation on helical structures, *Proc. IRE*, Vol. 43, 149–161, 1955.

18. HFSS10.0 User's Manual, Ansoft Corporation, Pittsburgh.